

# Temperature-Dependent Optical Constants of Nanometer-thin Flakes of Fe(Te,Se) Superconductor in the Visible and Near-Infrared Regime

Aswini K. Pattanayak, Jagi Rout, and Pankaj K. Jha\*

*Quantum Technology Laboratory (Q|T|L),*

*Department of Electrical Engineering and Computer Science,*

*Syracuse University, Syracuse, NY 13244, USA*

(Dated: July 22, 2024)

## Abstract

Iron chalcogenides superconductors, such as Fe(Te,Se) have recently garnered significant attention due to their simple crystal structure with a relatively easy synthesis process, high-temperature superconductivity, intrinsic topological band structure, and an unconventional pairing of superconductivity with ferromagnetism. Here, we report the complex in-plane refractive index measurement of nanometer-thin Fe(Te,Se) flake exfoliated from a single crystal FeTe<sub>0.6</sub>Se<sub>0.4</sub> for photon wavelengths from 450 to 1100 nm over a temperature range from 4 K to 295 K. The results were obtained by employing a two-Drude model for the dielectric function of Fe(Te,Se), a multiband superconductor, and fitting the absolute optical reflection spectra using the transfer matrix method. A high extinction coefficient in the visible to near-infrared range makes nanometer-thin Fe(Te,Se) flakes a promising material for photodetection applications.

---

\* Correspondence and requests for materials should be requested to P.K.J (pkjha@syr.edu)

The discovery of iron-based superconductors (IBS)  $\text{La}[\text{O}_{1-x}\text{F}_x]\text{FeAs}$  in 2008 [1], with the superconducting critical transition temperature  $T_c$  of 26 K, introduced a new family of high-temperature superconductors besides copper-based materials [2]. Soon, it was demonstrated that  $T_c$  can be elevated to  $\sim 50$  K in similar compounds by replacing Lanthanum (La) with rare-earth elements Cerium (Ce) [3], Neodymium (Nd) [4], Praseodymium (Pr) [5] or Samarium (Sm) [6]. Similar to cuprates, the superconductivity in IBS has an unconventional origin associated with spin fluctuations rather than the conventional electron-phonon pairing mechanism [7, 8]. Within the family of IBS, layered iron-chalcogenides such as FeSe (so-called “11-phase”) have served as a key material to understanding the microscopic physics of unconventional superconductivity in IBS owing to their simple crystal structure, relatively straightforward synthesis process, and lower toxicity stemming from the absence of the toxic heavy metal arsenic (As). Although for bulk FeSe single crystal at ambient pressure, the  $T_c = 8\text{K}$  [9] is relatively low for a high-temperature superconductor. By doping FeSe with tellurium (Te) [10–12] i.e.,  $\text{FeTe}_x\text{Se}_{1-x}$  ( $0 \leq x \leq 1$ ), hereafter referred to as Fe(Te,Se),  $T_c$  can be increased due to expansion of the lattice parameters and reaches up to 15.2 K at a concentration of about  $x \sim 0.5$ . However, a further increase in Te concentration in Fe(Te,Se) lowers its  $T_c$  due to the strengthening of antiferromagnetic ordering. In the extreme limit,  $x = 1$ , superconductivity vanishes, i.e., bulk FeTe is not superconducting.

Recently, Fe(Te,Se) has stimulated great interest owing to its inherent unconventional pairing of superconductivity with ferromagnetism [13], observation of exotic high-temperature topological superconductivity [14, 15] and Majorana bound states [16, 17]. Remarkably, analogous to its parent compound FeSe, monolayer Fe(Te,Se) on  $\text{SrTiO}_3$  exhibits interfaced-enhanced  $T_c$  of 40 K [18]. In the normal (non-superconducting) state, Fe(Te,Se) is a bad metal due to strong electron correlation [19–21]. The optical conductivity measurement indicates a significant reduction in the Drude weight due to electron correlations, providing evidence of bad metal behavior. Furthermore, electronic structure calculations [22] and angle-resolved photoemission spectroscopy [23–25] reveal that Fe(Te,Se) is a multiband superconductor. The band structure of Fe(Te,Se) consists of the hole bands at the  $\Gamma$  point and the electron bands at the M point [26, 27], and its optical properties are best described by the two-Drude model for dielectric function [28–32]. Fe(Te,Se) has been extensively studied for its magnetic properties; however, the optical properties of nanometer-thin films or flakes for photonic applications in visible to near-IR wavelengths over a wide range of temperatures remain relatively unexplored.

In this Letter, we present the measurement of the complex-valued in-plane refractive index

$\tilde{n} = n + ik$  of nanometer-thin Fe(Te,Se) flake exfoliated from a single crystal FeTe<sub>0.6</sub>Se<sub>0.4</sub> onto a SiO<sub>2</sub>/Si substrate over the 450 to 1100 nm wavelength range from 4 K to 295 K. We obtained the complex refractive index  $\tilde{n}$  by employing the two-Drude band model for the dielectric function and use the transfer matrix method [33] to fit thickness-dependent absolute reflection spectra from Fe(Te,Se)/SiO<sub>2</sub>/Si stack. At 4 K, the refractive index and extinction coefficient vary in the range of 2.81 - 4.26 and 2.24 - 3.21, respectively. In the normal state (295 K), they vary between 2.79 - 4.38 and 2.14 - 3.04. The two-Drude model reveals a stronger Drude component  $\omega_{p,1} \simeq 27763$  cm<sup>-1</sup> and the scattering rate  $\gamma_1 \simeq 2521$  cm<sup>-1</sup> at 4K. The other Drude component  $\omega_{p,2} \simeq 3184$  cm<sup>-1</sup>, with a weaker scattering rate  $\gamma_2 \simeq 93$  cm<sup>-1</sup> at 4K, which increases to  $\simeq 950$  cm<sup>-1</sup> at 295 K.

Figure 1 shows the experimental configuration of the optical reflectance measurement. A nanometer-thin flake of Fe(Te,Se) was exfoliated from the bulk single crystal FeTe<sub>0.6</sub>Se<sub>0.4</sub> using the conventional scotch-tape method [34] and transferred to a SiO<sub>2</sub>/Si substrate. An optical image of the flake under study is shown in Fig. 1(inset, lower left panel (b)), where the color variation across the flake depends both on the number of layers and on the thickness of SiO<sub>2</sub> layer. Here, the thickness of SiO<sub>2</sub> is 278 nm. The crystal structure of Fe(Te,Se), as shown in Fig. 1(inset, right panel (a)), is composed of a stack of Fe, Te/Se layers where a square lattice of Fe atoms is sandwiched between two Se/Te layers. The interlayer coupling is crucial for the electronic and magnetic properties of Fe(Te,Se). The lattice constant along the *c*-axis is 6.1 Å, while 3.8 Å in the *a*-*b* plane. For the reflectance measurements, the sample was illuminated using broadband emission from a tungsten halogen light source, which was then focused onto the sample using an objective (NA = 0.8) with a spot size of 3 μm. The same objective collected the reflected light and directed it to a spectrometer with a spectral resolution of 1 nm using a beam splitter. Only the *in-plane* refractive index is measured in our experimental configuration as the optical fields lie in the sample plane. To determine the thickness of the exfoliated flake, we employed atomic force microscopy (AFM). Figure 1 (inset, upper left panel (c)) shows an AFM image of the Fe(Te,Se) flake under study and the height profile across the vertical line. From the height profile, we extracted the height of the flake as 7.6 nm, corresponding to  $\sim 12$ -layers.

We performed Raman spectroscopy to identify Fe(Te,Se) flakes using a confocal inVia Raman microscope with an excitation laser wavelength of 532 nm. A 50X objective microscope lens was utilized to focus the laser beam on the flake. The acquisition time was set to 5 seconds to achieve well-resolved peaks. We probed different sample locations to ensure the spectra' repeatability.

Figure 2(a) shows the room-temperature Raman spectra in low wavenumber range 100 - 550  $\text{cm}^{-1}$  for 7.6 nm flake. In the range 100 - 250  $\text{cm}^{-1}$ , this thick flake exhibits two peaks  $P_{1,2}$  at  $155.6 \pm 0.1 \text{ cm}^{-1}$  and  $203.8 \pm 0.7 \text{ cm}^{-1}$  with a linewidth of  $34.8 \pm 0.5 \text{ cm}^{-1}$  and  $20.1 \pm 2.6 \text{ cm}^{-1}$ , respectively. These peaks  $P_{1,2}$  have been attributed to the  $A_{1g}$  mode associated with the out-of-plane vibration for Te/Se and the  $B_{1g}$  mode for the Fe atom vibrations along the  $c$ -axis, respectively. Okazaki *et al.* observed  $A_{1g}$  and  $B_{1g}$  modes of  $\text{FeTe}_{0.6}\text{Se}_{0.4}$  at  $161 \text{ cm}^{-1}$  and  $202 \text{ cm}^{-1}$ , respectively [35]. However, large discrepancies have been observed in the literature [36–38] regarding the exact positions of these peaks. For instance, Lopes *et al.* reported similar Raman shifts at  $120 \pm 1 \text{ cm}^{-1}$  and  $139 \pm 1 \text{ cm}^{-1}$  in  $\text{FeTe}_{0.5}\text{Se}_{0.5}$  sample [36]. Figure 2(b) shows the Raman spectra from 7.6 nm and 17 nm thick regions of the same flake under identical excitation power, integration time, and temperature conditions. As the thickness of the flakes increases to 17.0 nm, the position of  $A_{1g}$  mode does not show any variation; however, the position of  $B_{1g}$  mode is red-shifted to  $195.6 \pm 0.2 \text{ cm}^{-1}$ . Furthermore, the linewidth of  $B_{1g}$  mode reduces by more than two-fold for the 17 nm thick flake compared to the 7.6 nm flake. The spectral feature at  $\sim 300 \text{ cm}^{-1}$  and  $\sim 520 \text{ cm}^{-1}$  in Fig. 2(a,b) are associated with silicon substrate.

Figure 3(a,d) shows the absolute reflectance spectra of our heterostructure stack  $\text{Fe}(\text{Te},\text{Se})/\text{SiO}_2/\text{Si}$  at 4 K and 295 K, respectively. The value of absolute reflectance reaches 0.4 for a wider range from 700 nm to 900 nm; a strong absorption dip observed from 500 nm to 600 nm might be attributed to a strong absorption in this range. Next, to extract the complex refractive index  $\tilde{n} = \sqrt{\tilde{\epsilon}} = n + ik$ , we employed the two-Drude model to describe the complex dielectric function of  $\text{Fe}(\text{Te},\text{Se})$  [28–32] and used transfer matrix method [33] to fit thickness-dependent absolute reflection spectra. In the two-Drude model, the complex dielectric function is described by the standard Drude-Lorentz oscillator model [40] with two Drude terms as follows:

$$\tilde{\epsilon}(\omega) = \epsilon_{\infty} - \frac{\omega_{p,1}^2}{\omega^2 + i\omega\gamma_1} - \frac{\omega_{p,2}^2}{\omega^2 + i\omega\gamma_2} + \sum_j \frac{\Omega_j^2}{\omega_j^2 - \omega^2 - i\omega\Gamma_j} \quad (1)$$

where  $\epsilon_{\infty}$  is the real part at high frequency,  $\omega_{p,1(2)}$  and  $\Gamma_{1(2)}$  are the plasma frequency and scattering rates for the Drude carriers, respectively. Contributions from the  $j^{\text{th}}$ -bound excitations is quantified by the parameters  $\Omega_j$  (strength),  $\omega_j$  (position), and  $\Gamma_j$  (width). We used the dielectric function of Eq. (1) with two Lorentzian terms to fit the measured absolute reflectance data by varying the model parameters to match the experimental data. Figure 3(a,d) shows the experimental data (black line) and the fitting curve (red line). From the fitting, we obtained the parameters of two Drude components ( $\omega_{p,1/2}, \gamma_{1/2}$ ) as:  $\omega_{p,1} \simeq 27736 \text{ cm}^{-1}$ ,  $\gamma_1 \simeq 2512 \text{ cm}^{-1}$  and  $\omega_{p,2} \simeq 3184$

$\text{cm}^{-1}$ ,  $\gamma_2 \simeq 93 \text{ cm}^{-1}$  at 4 K. Similar to its parent compound FeSe, the broad Drude band ( $\omega_{p,1}, \gamma_1$ ) dominates the spectral weight ( $(\omega_{p,1}/\omega_{p,2})^2 \gg 1$ ) compared to the narrower band ( $\omega_{p,2}, \gamma_2$ ) and the overall plasma frequency  $\omega_p = (\omega_{p,1}^2 + \omega_{p,2}^2)^{1/2} \approx 27918 \text{ cm}^{-1}$ . At 295 K, those parameters become  $\omega_{p,1} \simeq 26672 \text{ cm}^{-1}$ ,  $\gamma_1 \simeq 3752 \text{ cm}^{-1}$  and  $\omega_{p,2} \simeq 1000 \text{ cm}^{-1}$ ,  $\gamma_2 \simeq 950 \text{ cm}^{-1}$ . Figures 3(b-f) show the refractive index and extinction coefficient of Fe(Te,Se) for photon wavelengths from 450 to 1100 nm at 4 K and 295 K. We observed both normal ( $dn/d\lambda < 0$ ) and abnormal ( $dn/d\lambda > 0$ ) dispersion in Fe(Te,Se) within specific spectral range. The refractive index and the extinction coefficient vary in the range of 2.81 - 4.26 and 2.24 - 3.21, respectively, at 4 K. At 295 K, they vary in the range of 2.79 - 4.38 and 2.14 - 3.04. In particular, at 800 nm, we have  $k = 2.97$  at 295 K. On the other hand, for the parent compound FeSe on  $\text{CaF}_2$  substrate  $k = 2.33$  [41]. A higher extinction coefficient of Fe(Te,Se) is advantageous for photodetection applications [42]. To compare other high- $T_c$  superconductors with Fe(Te,Se), we have studied optical constants for  $\text{Bi}_2\text{Sr}_2\text{CaCu}_2\text{O}_{8+\delta}$  (BSCCO) at 295 K (See supporting information Fig S8). In the entire spectral range (450 -1100 nm), the extinction coefficient for Fe(Te,Se) is higher than BSCCO, thus making it a promising candidate for high-temperature single-photon detectors.

Next, we studied the temperature-dependent reflection spectra of the flake from 4 K to 295 K for photon wavelengths from 450 to 1100 nm. The plot for differential reflectivity  $\Delta(\mathcal{R})$  of Fe(Te,Se) defined as

$$\Delta(\mathcal{R}) = \frac{\mathcal{R}_{\text{Fe(Te,Se)}} - \mathcal{R}_{\text{SiO}_2/\text{Si}}}{\mathcal{R}_{\text{SiO}_2/\text{Si}}} \quad (2)$$

is presented in Supporting information (See section S3). Figure 4(a,b) plots the temperature-dependent refractive index and extinction coefficient from 4 K to 295 K, with a 0.2 offset on the  $y$ -axis for visual clarity. With increasing temperature, we have observed a blue shift in oscillator position at low energy ( $\approx 450 \text{ nm}$ ). For instance, a blue shift of  $\approx 11 \text{ nm}$  in the position of the refractive index peak at 10 K ( $\lambda \approx 482 \text{ nm}$ ) compared to 4 K ( $\lambda \approx 493 \text{ nm}$ ) and the corresponding change  $\Delta n = n_{10\text{K}} - n_{4\text{K}} \approx 0.011$ . Similarly, a blue shift of  $\approx 11 \text{ nm}$  in the position of the extinction coefficient minima at 10 K ( $\lambda \approx 542 \text{ nm}$ ) compared to 4 K ( $\lambda \approx 553 \text{ nm}$ ) and the corresponding change  $\Delta k = k_{10\text{K}} - k_{4\text{K}} \approx 0.067$ . The variation of plasma frequencies  $\omega_{p,1}$  and  $\omega_{p,2}$  and the scattering rates  $\Gamma_1$  and  $\Gamma_2$  has been presented in Supporting Information S4. We observed that the plasma frequency and scattering terms for both the broad and narrow components show little to no variation up to 70 K for Fe (Te,Se) apart from a strong narrow component  $\omega_{p,2}$  4 K for Fe(Te,Se). On the other hand, the scattering rate for the narrow component  $\Gamma_2$  gradually increases with temperature. At 295 K, it reaches about a quarter of the  $\Gamma_2$  value and is an order of

magnitude greater than its value at 4 K.

In summary, we report the measurement of the complex-valued in-plane refractive index  $\tilde{n} = n + ik$  of nanometer-thin flakes of multiband superconductor Fe(Te,Se) over the 450 to 1100 nm wavelength range from 4 K to 295 K. We obtained the complex refractive index  $\tilde{n}$  by employing the two-Drude band model and the transfer matrix method to fit thickness-dependent reflection spectra from our heterostructure stack Fe(Te,Se)/SiO<sub>2</sub>/Si. In room-temperature Raman spectra, we observed two peaks P<sub>1,2</sub> at  $155.6 \pm 0.1 \text{ cm}^{-1}$  and  $203.8 \pm 0.7 \text{ cm}^{-1}$  with a linewidth of  $34.8 \pm 0.5 \text{ cm}^{-1}$  and  $20.1 \pm 2.6 \text{ cm}^{-1}$ , respectively. These peaks P<sub>1,2</sub> have been attributed to the A<sub>1g</sub> mode for Te/Se and the B<sub>1g</sub> mode for the Fe atom vibrations, respectively. For a thicker (17.0 nm) flake, we observed B<sub>1g</sub> mode is red-shifted by  $8.2 \pm 0.7 \text{ cm}^{-1}$  but no noticeable change in the position of A<sub>1g</sub> mode compared to 7.6 nm Fe(Te,Se) flake. In the superconducting state (4 K), the refractive index and the extinction coefficient vary in the range of 2.81 - 4.26 and 2.24 - 3.21, respectively. In the normal state (295 K), they vary between 2.79 - 4.38 and 2.14 - 3.04. Our temperature-dependent reflection spectra yield a stronger and broader Drude response  $\omega_{p,1} \simeq 27736 \text{ cm}^{-1}$ , with a significant scattering rate  $\gamma_1 \simeq 2512 \text{ cm}^{-1}$  that is essentially independent of temperature at the low-temperature regime. The other Drude response  $\omega_{p,2} \simeq 3184 \text{ cm}^{-1}$ , with weaker scattering rate  $\gamma_2 \simeq 93 \text{ cm}^{-1}$  which increases by an order of magnitude to  $\simeq 950 \text{ cm}^{-1}$ . The detailed optical properties reported here over a large range of temperatures in the visible and near-IR regime could open new photonics and quantum photonics applications of Fe(Te, Se).

### Supplementary Material

Experimental setup, AFM Measurement for 17 nm Fe(Te,Se) flake, differential reflectivity for 7.6 nm thin Fe(Te,Se) flake, temperature-dependence of Drude parameters for 7.6 nm Fe(Te,Se) flake, absolute reflectance for 17 nm and 7.6 nm Fe(Te,Se) flake, complex refractive index for 17 nm Fe(Te,Se) flake at 4 K and 295 K, absolute reflectance and coefficients of complex refractive index for BSCCO, fitting parameters (Lorentz-oscillators) for 7.6 nm flake.

### DATA AVAILABILITY

The data that support the findings of this study are available within the article (and its supplementary material)

- 
- [1] Y. Kamihara, T. Watanabe, M. Hirano, and H. Hosono, “Iron-Based Layered Superconductor  $\text{La}[\text{O}_{1-x}\text{F}_x]\text{FeAs}$  ( $x=0.05 - 0.12$ ) with  $T_c = 26$  K,” *J. Am. Chem. Soc.* 130(11), 3296–3297 (2008).
- [2] J.G. Bednorz, and K.A. Müller, “Possible high  $T_c$  superconductivity in the barium-lanthanum-copper-oxygen system,” *Z. Physik B - Condensed Matter* 64(2), 189–193 (1986).
- [3] G.F. Chen, Z. Li, D. Wu, G. Li, W.Z. Hu, J. Dong, P. Zheng, J.L. Luo, and N.L. Wang, “Superconductivity at 41 K and Its Competition with Spin-Density-Wave Instability in Layered  $\text{CeO}_{1-x}\text{F}_x\text{FeAs}$ ,” *Phys. Rev. Lett.* 100(24), 247002 (2008).
- [4] Z.-A. Ren, J. Yang, W. Lu, W. Yi, X.-L. Shen, Z.-C. Li, G.-C. Che, X.-L. Dong, L.-L. Sun, F. Zhou, and Z.-X. Zhao, “Superconductivity in the iron-based F-doped layered quaternary compound  $\text{Nd}[\text{O}_{1-x}\text{F}_x]\text{FeAs}$ ,” *EPL* 82(5), 57002 (2008).
- [5] Z.A. Ren, J. Yang, W. Lu, W. Yi, G.C. Che, X.L. Dong, L.L. Sun, and Z.X. Zhao, “Superconductivity at 52 K in iron based F doped layered quaternary compound  $\text{Pr}[\text{O}_{1-x}\text{F}_x]\text{FeAs}$ ,” *Materials Research Innovations* 12(3), 105–106 (2008).
- [6] R. Zhi-An, L. Wei, Y. Jie, Y. Wei, S. Xiao-Li, Zheng-Cai, C. Guang-Can, D. Xiao-Li, S. Li-Ling, Z. Fang, and Z. Zhong-Xian, “Superconductivity at 55 K in Iron-Based F-Doped Layered Quaternary Compound  $\text{Sm}[\text{O}_{1-x}\text{F}_x]\text{FeAs}$ ,” *Chinese Phys. Lett.* 25(6), 2215 (2008).
- [7] P.J. Hirschfeld, M.M. Korshunov, and I.I. Mazin, “Gap symmetry and structure of Fe-based superconductors,” *Rep. Prog. Phys.* 74(12), 124508 (2011).
- [8] D.J. Scalapino, “The case for  $d_{x^2-y^2}$  pairing in the cuprate superconductors,” *Physics Reports* 250(6), 329–365 (1995).
- [9] F.-C. Hsu, J.-Y. Luo, K.-W. Yeh, T.-K. Chen, T.-W. Huang, P.M. Wu, Y.-C. Lee, Y.-L. Huang, Y.-Y. Chu, D.-C. Yan, and M.-K. Wu, “Superconductivity in the PbO-type structure  $\alpha$ -FeSe,” *Proceedings of the National Academy of Sciences* 105(38), 14262–14264 (2008).
- [10] K.-W. Yeh, T.-W. Huang, Y. Huang, T.-K. Chen, F.-C. Hsu, P.M. Wu, Y.-C. Lee, Y.-Y. Chu, C.-L. Chen, J.-Y. Luo, D.-C. Yan, and M.-K. Wu, “Tellurium substitution effect on superconductivity of the  $\alpha$ -phase iron selenide,” *EPL* 84(3), 37002 (2008).
- [11] M.H. Fang, H.M. Pham, B. Qian, T.J. Liu, E.K. Vehstedt, Y. Liu, L. Spinu, and Z.Q. Mao, “Superconductivity close to magnetic instability in  $\text{FeTe}_x(\text{Se}_{1-x})_{0.82}$ ,” *Phys. Rev. B* 78(22), 224503 (2008).
- [12] K. W. Yeh, H. C. Hsu, T. W. Huang, P. M. Wu, Y. L. Huang, T. K. Chen, J. Y. Luo, and M. K. Wu, “Se

- and Te Doping Study of the FeSe Superconductors,” J. Phys. Soc. Jpn. 77(Suppl.C), 19–22 (2008).
- [13] J. Paglione, and R.L. Greene, “High-temperature superconductivity in iron-based materials,” Nature Phys 6(9), 645–658 (2010).
- [14] J.D. Rameau, N. Zaki, G.D. Gu, P.D. Johnson, and M. Weinert, “Interplay of paramagnetism and topology in the Fe-chalcogenide high- $T_c$  superconductors,” Phys. Rev. B 99(20), 205117 (2019).
- [15] P. Zhang, Z. Wang, X. Wu, K. Yaji, Y. Ishida, Y. Kohama, G. Dai, Y. Sun, C. Bareille, K. Kuroda, T. Kondo, K. Okazaki, K. Kindo, X. Wang, C. Jin, J. Hu, R. Thomale, K. Sumida, S. Wu, K. Miyamoto, T. Okuda, H. Ding, G.D. Gu, T. Tamegai, T. Kawakami, M. Sato, and S. Shin, “Multiple topological states in iron-based superconductors,” Nature Phys 15(1), 41–47 (2019).
- [16] L. Kong, S. Zhu, M. Papaj, H. Chen, L. Cao, H. Isobe, Y. Xing, W. Liu, D. Wang, P. Fan, Y. Sun, S. Du, J. Schneeloch, R. Zhong, G. Gu, L. Fu, H.-J. Gao, and H. Ding, “Half-integer level shift of vortex bound states in an iron-based superconductor,” Nat. Phys. 15(11), 1181–1187 (2019).
- [17] D. Wang, L. Kong, P. Fan, H. Chen, S. Zhu, W. Liu, L. Cao, Y. Sun, S. Du, J. Schneeloch, R. Zhong, G. Gu, L. Fu, H. Ding, and H.-J. Gao, “Evidence for Majorana bound states in an iron-based superconductor,” Science 362(6412), 333–335 (2018).
- [18] F. Li, H. Ding, C. Tang, J. Peng, Q. Zhang, W. Zhang, G. Zhou, D. Zhang, C.-L. Song, K. He, S. Ji, X. Chen, L. Gu, L. Wang, X.-C. Ma, and Q.-K. Xue, “Interface-enhanced high-temperature superconductivity in single-unit-cell  $\text{FeTe}_x\text{Se}_{1-x}$  films on  $\text{SrTiO}_3$ ,” Phys. Rev. B 91(22), 220503 (2015).
- [19] B.C. Sales, A.S. Sefat, M.A. McGuire, R.Y. Jin, D. Mandrus, and Y. Mozharivskyj, “Bulk superconductivity at 14 K in single crystals of  $\text{Fe}_{1-y}\text{Te}_x\text{Se}_{1-x}$ ,” Phys. Rev. B 79(9), 094521 (2009).
- [20] A. Pourret, L. Malone, A.B. Antunes, C.S. Yadav, P.L. Paulose, B. Fauqué, and K. Behnia, “Strong correlation and low carrier density in  $\text{Fe}_{1-y}\text{Te}_{0.6}\text{Se}_{0.4}$  as seen from its thermoelectric response,” Phys. Rev. B 83(2), 020504 (2011).
- [21] N. Lanatà, H.U.R. Strand, G. Giovannetti, B. Hellsing, L. de’ Medici, and M. Capone, “Orbital selectivity in Hund’s metals: The iron chalcogenides,” Phys. Rev. B 87(4), 045122 (2013).
- [22] A. Subedi, L. Zhang, D.J. Singh, and M.H. Du, “Density functional study of FeS, FeSe, and FeTe: Electronic structure, magnetism, phonons, and superconductivity,” Phys. Rev. B 78(13), 134514 (2008).
- [23] F. Chen, B. Zhou, Y. Zhang, J. Wei, H.-W. Ou, J.-F. Zhao, C. He, Q.-Q. Ge, M. Arita, K. Shimada, H. Namatame, M. Taniguchi, Z.-Y. Lu, J. Hu, X.-Y. Cui, and D.L. Feng, “Electronic structure of



- $\text{Fe}_{1.04}\text{Te}_{0.66}\text{Se}_{0.34}$ ,” *Phys. Rev. B* 81(1), 014526 (2010).
- [24] A. Tamai, A.Y. Ganin, E. Rozbicki, J. Bacsá, W. Meevasana, P.D.C. King, M. Caffio, R. Schaub, S. Margadonna, K. Prassides, M.J. Rosseinsky, and F. Baumberger, “Strong Electron Correlations in the Normal State of the Iron-Based  $\text{FeSe}_{0.42}\text{Te}_{0.58}$  Superconductor Observed by Angle-Resolved Photoemission Spectroscopy,” *Phys. Rev. Lett.* 104(9), 097002 (2010).
- [25] P. Zhang, P. Richard, N. Xu, Y.-M. Xu, J. Ma, T. Qian, A.V. Fedorov, J.D. Denlinger, G.D. Gu, and H. Ding, “Observation of an electron band above the Fermi level in  $\text{FeTe}_{0.55}\text{Se}_{0.45}$  from in-situ surface doping,” *Applied Physics Letters* 105(17), 172601 (2014).
- [26] H. Miao, P. Richard, Y. Tanaka, K. Nakayama, T. Qian, K. Umezawa, T. Sato, Y.-M. Xu, Y.B. Shi, N. Xu, X.-P. Wang, P. Zhang, H.-B. Yang, Z.-J. Xu, J.S. Wen, G.-D. Gu, X. Dai, J.-P. Hu, T. Takahashi, and H. Ding, “Isotropic superconducting gaps with enhanced pairing on electron Fermi surfaces in  $\text{FeTe}_{0.55}\text{Se}_{0.45}$ ,” *Phys. Rev. B* 85(9), 094506 (2012).
- [27] K. Nakayama, R. Tsubono, G.N. Phan, F. Nabeshima, N. Shikama, T. Ishikawa, Y. Sakishita, S. Ideta, K. Tanaka, A. Maeda, T. Takahashi, and T. Sato, “Orbital mixing at the onset of high-temperature superconductivity in  $\text{FeTe}_x\text{Se}_{1-x}/\text{CaF}_2$ ,” *Phys. Rev. Res.* 3(1), L012007 (2021).
- [28] C.C. Homes, A. Akrap, J.S. Wen, Z.J. Xu, Z.W. Lin, Q. Li, and G.D. Gu, “Electronic correlations and unusual superconducting response in the optical properties of the iron chalcogenide  $\text{FeTe}_{0.55}\text{Se}_{0.45}$ ,” *Phys. Rev. B* 81(18), 180508 (2010).
- [29] C.C. Homes, A. Akrap, J. Wen, Z. Xu, Z. Wei Lin, Q. Li, and G. Gu, “Optical properties of the iron-chalcogenide superconductor  $\text{FeTe}_{0.55}\text{Se}_{0.45}$ ,” *Journal of Physics and Chemistry of Solids* 72(5), 505–510 (2011).
- [30] A. Pimenov, S. Engelbrecht, A.M. Shuvaev, B.B. Jin, P.H. Wu, B. Xu, L.X. Cao, and E. Schachinger, “Terahertz conductivity in  $\text{FeSe}_{0.5}\text{Te}_{0.5}$  superconducting films,” *New J. Phys.* 15(1), 013032 (2013).
- [31] A. Perucchi, B. Joseph, S. Caramazza, M. Autore, E. Bellingeri, S. Kawale, C. Ferdeghini, M. Putti, S. Lupi, and P. Dore, “Two-Band Conductivity of a  $\text{FeSe}_{0.5}\text{Te}_{0.5}$  Film by Reflectance Measurements in the Terahertz and Infrared Range,” *Supercond. Sci. Technol.* 27(12), 125011 (2014).
- [32] C.C. Homes, Y.M. Dai, J.S. Wen, Z.J. Xu, and G.D. Gu, “ $\text{FeTe}_{0.55}\text{Se}_{0.45}$ : A multiband superconductor in the clean and dirty limit,” *Phys. Rev. B* 91(14), 144503 (2015).
- [33] H.A. Macleod, *Thin-Film Optical Filters*, Fourth Edition (Taylor Francis, 2010).
- [34] Y. Huang, E. Sutter, N.N. Shi, J. Zheng, T. Yang, D. Englund, H.-J. Gao, and P. Sutter, “Reliable Exfoliation of Large-Area High-Quality Flakes of Graphene and Other Two-Dimensional Materials,”

- ACS Nano 9(11), 10612–10620 (2015).
- [35] K. Okazaki, S. Sugai, S. Niitaka, and H. Takagi, “Phonon, two-magnon, and electronic Raman scattering of  $\text{Fe}_{1+y}\text{Te}_{1-x}\text{Se}_x$ ,” *Phys. Rev. B* 83(3), 035103 (2011).
- [36] C.S. Lopes, C.E. Foerster, F.C. Serbena, P.R. Júnior, A.R. Jurelo, J.L.P. Júnior, P. Pureur, and A.L. Chinelatto, “Raman spectroscopy of highly oriented  $\text{FeSe}_{0.5}\text{Te}_{0.5}$  superconductor,” *Supercond. Sci. Technol.* 25(2), 025014 (2012).
- [37] T.-L. Xia, D. Hou, S.C. Zhao, A.M. Zhang, G.F. Chen, J.L. Luo, N.L. Wang, J.H. Wei, Z.-Y. Lu, and Q.M. Zhang, “Raman phonons of  $\alpha$ -FeTe and  $\text{Fe}_{1.03}\text{Se}_{0.3}\text{Te}_{0.7}$  single crystals,” *Phys. Rev. B* 79(14), 140510 (2009).
- [38] P.D. Lodhi, V.P.S. Awana, and N. Kaurav, “Raman and X-Ray Diffraction Studies of Superconducting  $\text{FeTe}_{1-x}\text{Se}_x$  Compounds,” *J. Phys.: Conf. Ser.* 836(1), 012046 (2017).
- [39] P. Kumar, A. Kumar, S. Saha, D.V.S. Muthu, J. Prakash, S. Patnaik, U.V. Waghmare, A.K. Ganguli, and A.K. Sood, “Anomalous Raman Scattering from Phonons and Electrons of Superconducting  $\text{FeSe}_{0.82}$ ,” *Solid State Communications* 150(13), 557–560 (2010).
- [40] M. Dressell and G. Grunner *Electrodynamics of Solids* (Cambridge: Cambridge University Press 2002)
- [41] S. Gerber, S.-L. Yang, D. Zhu, H. Soifer, J.A. Sobota, S. Rebec, J.J. Lee, T. Jia, B. Moritz, C. Jia, A. Gauthier, Y. Li, D. Leuenberger, Y. Zhang, L. Chaix, W. Li, H. Jang, J.-S. Lee, M. Yi, G.L. Dakovski, S. Song, J.M. Glowia, S. Nelson, K.W. Kim, Y.-D. Chuang, Z. Hussain, R.G. Moore, T.P. Devereaux, W.-S. Lee, P.S. Kirchmann, and Z.-X. Shen, “Femtosecond electron-phonon lock-in by photoemission and x-ray free-electron laser,” *Science* 357(6346), 71–75 (2017).
- [42] C.M. Natarajan, M.G. Tanner, and R.H. Hadfield, “Superconducting nanowire single-photon detectors: physics and applications,” *Supercond. Sci. Technol.* 25(6), 063001 (2012).

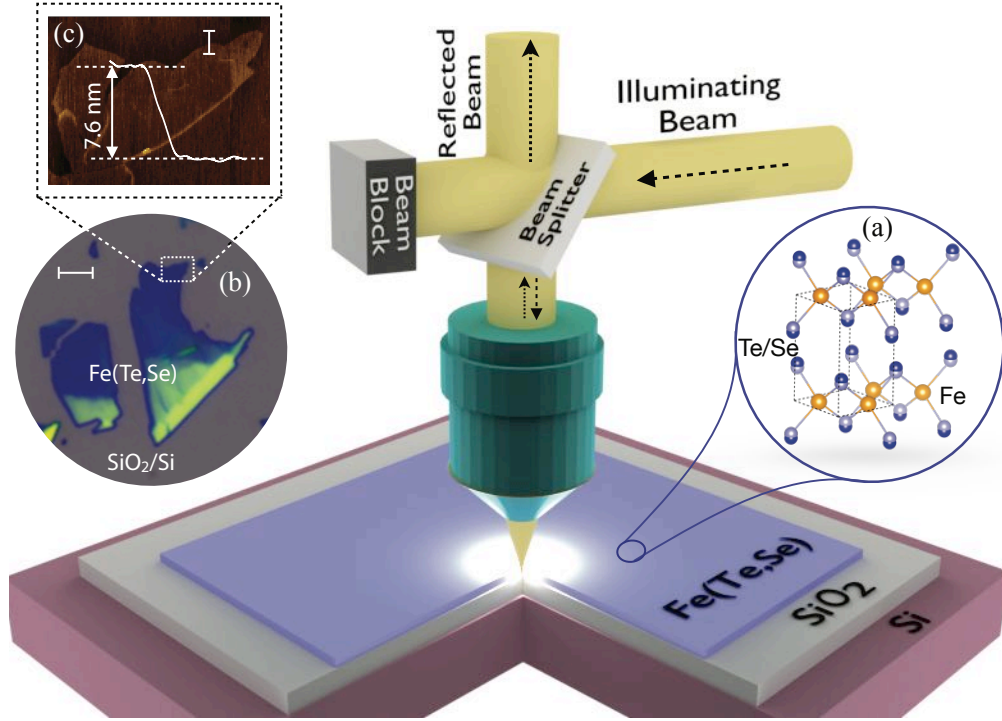


Figure 1: Experimental schematic and thickness characterization of Fe(Te,Se) flake. A nanometer-thin flake was exfoliated from a single crystal  $\text{FeTe}_{0.6}\text{Se}_{0.4}$  and transferred onto  $\text{SiO}_2/\text{Si}$  substrate using the conventional scotch-tape method. The thickness of the  $\text{SiO}_2$  layer is 278 nm. For our reflectance measurements, the same objective lens was used for broadband illumination and collection of the reflected light over the entire temperature range of 4 - 295 K. The lower right inset panel (a) shows the crystal structure of Fe(Te,Se) space group  $P4/nmm$  (No. 129), with room-temperature lattice parameters of  $a = b \approx 3.8 \text{ \AA}$ ,  $c \approx 6.1 \text{ \AA}$ . The lower left inset panel (b) shows the optical image of the flake of varying thicknesses used in this study. The upper left inset panel (c) shows an atomic force microscopy topography mapping of the flake. The vertical line trace gives a thickness of 7.6 nm which corresponds to  $\sim 12$  layers of the boxed region highlighted in (b).

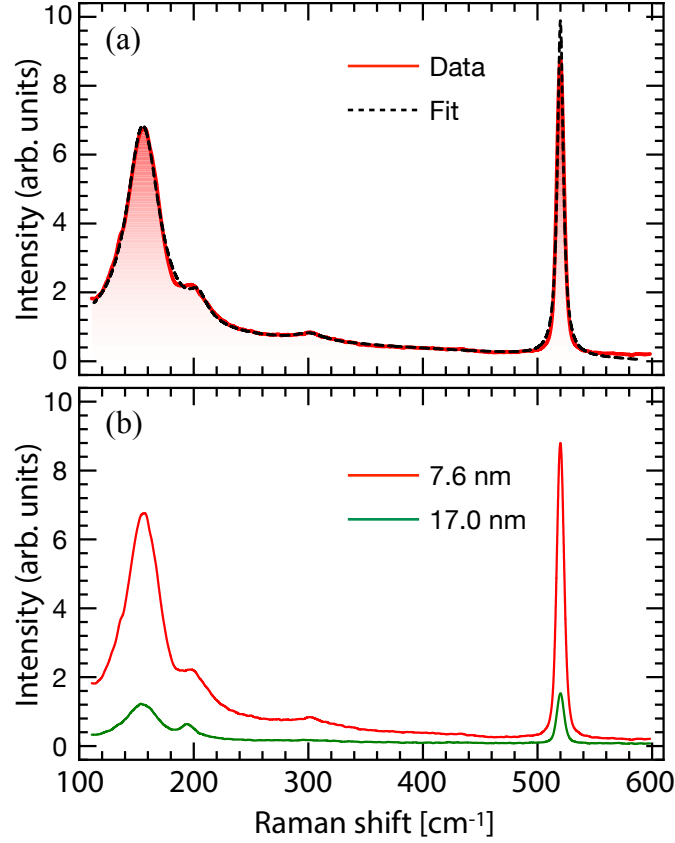


Figure 2: Room-temperature Raman spectroscopy of Fe(Te,Se) flakes. (a) Raman spectra for the 7.6 nm thin flake with multiple Lorentzian curve fitting. In the range 100 - 250 cm<sup>-1</sup>, the sample exhibits two peaks at  $155.6 \pm 0.1$  cm<sup>-1</sup> and  $203.8 \pm 0.7$  cm<sup>-1</sup> with a linewidth of  $34.8 \pm 0.5$  cm<sup>-1</sup> and  $20.1 \pm 2.6$  cm<sup>-1</sup> respectively. (b) Comparison of Raman spectra of 7.6 nm thin flake with 17.0 nm thin flake. With a thicker sample, we observed B<sub>1g</sub> mode is red-shifted by  $8.2 \pm 0.7$  cm<sup>-1</sup> but no noticeable change in the position of A<sub>1g</sub> mode. The spectral feature at  $\sim 300$  cm<sup>-1</sup> and  $\sim 520$  cm<sup>-1</sup> in Fig. 2(a,b) are associated with silicon substrate.

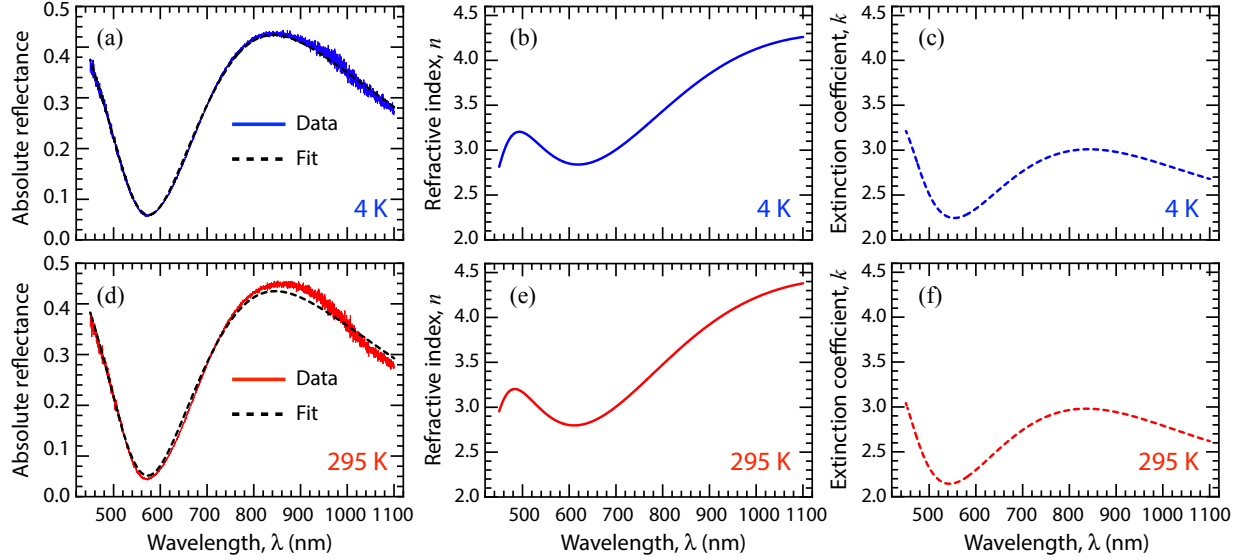


Figure 3: Optical constants of the Fe(Te,Se) flake at 4 K and 295 K. The plot of the absolute reflectance and fitted curve of the 7.6 nm thick Fe(Te,Se) flake at (a) 4K and (d) 295 K, respectively. The absolute reflectance was obtained by normalizing the sample's reflection spectra with the reflection spectra of a silver mirror. We fitted the measured reflectance spectra of our heterostructure stack Fe(Te,Se)/SiO<sub>2</sub>/Si using the transfer matrix method with the dielectric constant of Fe(Te,Se) given by Eq.(1). Plot of the calculated refractive index ( $n$ ) and the extinction coefficient ( $k$ ) of the Fe(Te,Se) flake at (b,c) 4K and (d,e) 295 K. Extinction coefficient, within our measurement window, at 295 K is 2.14 compared to 2.24 at 4 K. Similarly at 1100 nm the refractive index at 295 K is 4.38 which is higher than 4.26 at 4 K.

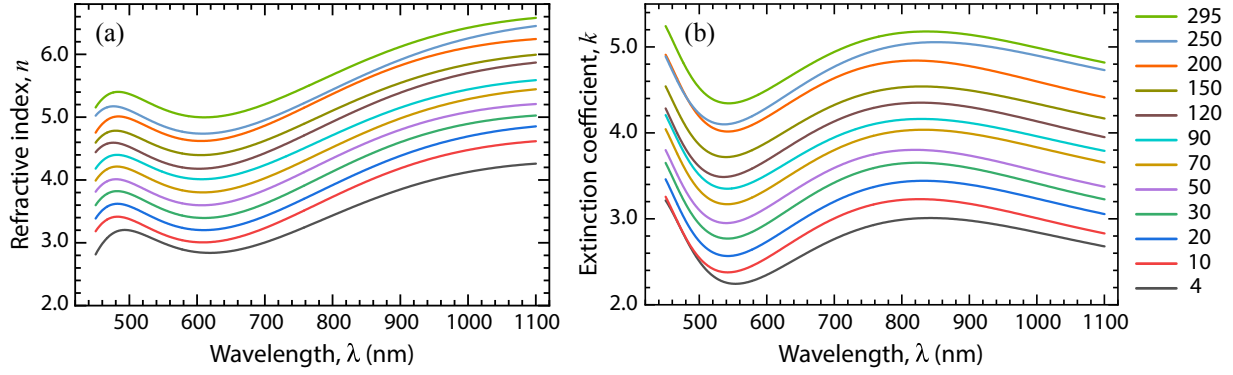


Figure 4: Temperature-dependent in-plane complex refractive index of Fe(Te,Se) flake. Plot of the (a) refractive index  $n$  and the (b) extinction coefficient  $k$  of the 7.6 nm thin Fe(Te,Se) flake against the wavelength at various temperatures. We observed a blue shift of  $\approx 11$  nm in the position of the refractive index peak at 10 K ( $\lambda \approx 482$  nm) compared to 4 K ( $\lambda \approx 493$  nm). Similarly, a blue shift of  $\approx 11$  nm in the position of the extinction coefficient minima at 10 K ( $\lambda \approx 542$  nm) compared to 4 K ( $\lambda \approx 553$  nm). The curves in both plots have been shifted vertically by 0.2 for visual clarity.